

A Multiobjective Optimization Framework for Strength and Stress Concentration in Variable Axial Composite Shells: A metaheuristic approach

Pedro Bühler Santana^{a*} , Herbert Martins Gomes^a , António Mendes Ferreira^c , Volnei Tita^{b,c} 

^aUniversidade Federal do Rio Grande do Sul, Departamento de Engenharia Mecânica, R. Sarmiento Leite, Porto Alegre, 90050-170, RS, Brasil.

E-mail: pedro.santana@ufrgs.br, herbert@mecanica.ufrgs.br

^bUniversidade de São Paulo, Escola de Engenharia de São Carlos, Departamento de Engenharia Aeronáutica, Av. João Dagnone, 1100 – Jardim Santa Angelina, 13563-120, São Carlos (SP), Brasil. E-mail: voltita@sc.usp.br

^cFaculdade de Engenharia da Universidade do Porto, Departamento de Engenharia Mecânica, Rua Dr. Roberto Frias s/n, 4200-465, Porto, Portugal. E-mail: ferreira@gcloud.fe.up.pt

* Corresponding author

<https://doi.org/10.1590/1679-78257577>

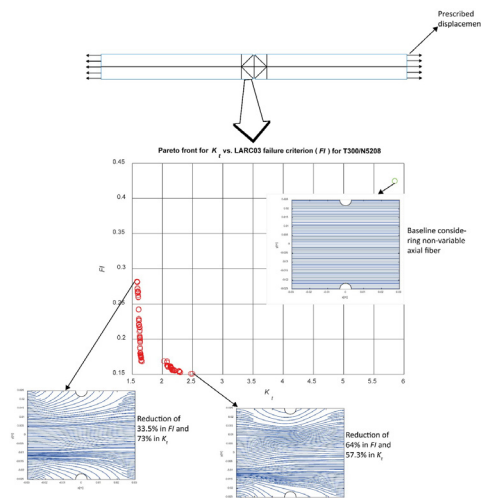
Abstract

A metaheuristic approach for variable axial composites considering multiobjective optimization is investigated. The proposed methodology is based on the combination of three main parts: a methodology for defining the orientation of the fibers in the laminate, a structural analysis program (based on the Finite Element Method) and an optimization algorithm. It is important to highlight that a radial basis function (RBF), which describes a smooth fiber pattern, is generated using control points. The novelties of the present methodology consist of a proposal for a generalized parameterization technique, which allows the investigation of mechanical strength and stress concentration of variable axial composites. Thus, NSGA-II multiobjective genetic algorithm is used as optimization tool to define the fiber orientations. Besides, a metaheuristic approach is used in situations when it is desirable to simultaneously minimize the stress concentration factor (K_t) and a failure criterion index (FI or Φ). Two case studies are investigated: a double notched plate and a tube with a transverse hole.

Keywords

Variable axial composites materials, composite materials, multiobjective optimization, stress analysis, finite element method.

Graphical Abstract



Received: March 15, 2023. In revised form: June 14, 2023. Accepted: June 16, 2023. Available online: June 20, 2023.

<https://doi.org/10.1590/1679-78257577>



Latin American Journal of Solids and Structures. ISSN 1679-7825. Copyright © 2023. This is an Open Access article distributed under the terms of the [Creative Commons Attribution License](https://creativecommons.org/licenses/by/4.0/), which permits unrestricted use, distribution, and reproduction in any medium, provided the original work is properly cited.

1 INTRODUCTION

Composite materials have been applied in fields where a high strength-weight ratio is required. They replace conventional materials in applications when such substitutions are feasible and show advantages like the improved strength, stiffness, fatigue and resistance to impact, (Kaw 2006).

It is common to find composite materials as laminate plates or shells, which are produced by using a lamination process. During the lamination is possible to tailor the directional dependence of strength and stiffness of a laminate to match the design loadings, which actuate in the composite structures (Jones 1999)

Usually, the laminas are reinforced by unidirectional fibers, which underestimate the potential of these materials in structural applications. However, due to the developments in robotics, new manufacturing processes such as TFP (Tailored Fiber Placement), AFP (Automated Fiber Placement), and CTS (Continuous Tow Shearing) have become a way to produce more optimized composite structures (Sobhani Aragh et al. 2021). These materials will be referred to as Variable Axial (VA) composites in the current paper, and their advantage is to steer the fibers to modify the stiffness and strength *in situ*. This allows, for example, adjusting the stiffness of a composite panel in order to increase its natural frequency (Guimarães et al. 2019). The CTS process is significantly outperformed by the TFP and AFP processes, where the similarity between the intended and produced components is better. The AFP process is a good choice for like-3D components, whereas the TFP has cheaper implementation cost and greater productivity. The main benefit of CTS is the layer deposition when compared to TFP. It is important to highlight that each kind of process can impose different restrictions in terms of fiber curvature that can be produced. However, in the present work, it was not considered any specific manufacturing process.

The efficiency of the resultant material is determined by the appropriate fiber trajectory, which must be established by the loads and requirements of the mechanical project. Depending on the field defined by the objective function, this optimal placement can be fairly complex. The current design approach relies upon a fiber direction parameterization technique in conjunction with an optimization algorithm. This methodology is found in many works in the literature since the ideal fiber trajectory is typically not obtained in a straightforward manner.

A common approach to parameterize the fiber placement is the use of a hypersurface to describe its angle at a given position. Honda et al. (2013) obtained the path of the fibers projecting over the finite elements mesh the tangential directions from the contour lines of a polynomial and use the mean curvature in conjunction with a failure criterion or the first modal frequency as objective functions in a multiobjective optimization framework. van Zanten et al. (2019) used a coarser manufacturing mesh as a hypersurface that has the angles of the fibers defined on its nodes. Through an inverse parametric transformation, these angles are interpolated to the centroids of elements, which describe the refined calculation mesh where displacement and stress components are evaluated. However, depending on the structure to be analyzed and on the complexity of the hypersurface, the optimization can present a high computational cost. Setoodeh et al. (2006) presents an alternative approach that uses lamination parameters to define the optimization problem with few design variables, which result in a convex space solution that allows to obtain a gradient optimization with fast convergence. Stodieck et al. (2017) also-applied lamination parameters as a base for their methodology using B-splines built from control points to describe the stiffness variation (via lamination parameters). Thus, a gradient-based optimization method (GCMMA) is used to identify the best value for buckling load. Finally, a genetic algorithm (GA) was used to extract curvilinear fiber paths from the target lamination parameters. Another technique to reduce the computational cost consists of replacing a burdensome structural analysis (as Finite Element Method - FEM) with a faster trained metamodel. Wang et al. (2020) developed a framework for axial buckling load optimization of VA composite cylinders using a reliability-based design optimization (RBDO) method, which takes the manufacturing parameters of the filament winding into account. The objective function of the optimization was the critical buckling load that is obtained through a Kriging metamodel trained with the results from finite element analysis. Almeida et al. (2019, 2021) evaluated the performance of VA cylinders (manufactured by filament winding) for buckling load, obtaining significant improvements in the implemented objective function, and discussing the effects of imperfections, thickness build-up and non-symmetric laminates on the buckling behavior.

The above-presented frameworks usually have as objective function some failure criterion, natural frequencies, buckling load considering a manufacturing constraint, but not approaching stress concentration. Regarding unidirectional composites, Ueng and Lin (1987) proposed solutions for plates with two elliptical holes under normal loads by combining analytical solutions for a plate with a hole with the superposition method applied to the stress potential functions. One of the findings of this research is that, in contrast to an isotropic material, stress patterns remain the same, but stress magnitude changes. Weixing and Xinlu (1991) showed solutions for stress concentration on unidirectional laminated composite plates using FEM, and the results were compared to the analytical solutions obtained by Chiang (1998).

However, for stress concentration analysis in Variable Axial (VA) composites, only few works are found in the literature. Vijayachandran and Waas (2022) studied the influence of steered fibers on the stress concentration around a hole in a laminate plate. The authors considered manufacturing parameters, and mechanical properties of the Robotic Automatic Fiber Placement (RAFP). A genetic algorithm was used as an optimizer, and reductions up to 33% in the stress concentration factor were obtained compared to a quasi-isotropic reference material.

Based on the aspects pointed out, in the present work, an investigation made by Santana et al. (2023) using a mono-objective optimization for mechanical strength is improved to a multiobjective optimization using the Non-Dominated Sorted Genetic Algorithm II (NSGA-II). It is important to highlight that, although this work presents some similarity to the previous one, the parameterization methods are essentially different. Control points (θ_{CP}) are dispersed over the finite element mesh, and angle orientation values are assigned to them. These angles are then interpolated to the integration points using Radial Basis Functions (RBF). The Cartesian coordinates of integration points are obtained by the use of the finite element shape functions, which allow change from the natural coordinate system to the Cartesian coordinate system. The objective functions are the stress concentration factor (Kt) and a failure criterion (Failure Index – FI). One case study consists of a notched plate that has been studied analytically by Weixing and Xinlu (1991) and numerically by {Chiang 1998} considering conventional (non-VA) composites reinforced by unidirectional fibers. In another case study, a composite tube is analyzed, observing the capability of the VA composite to reduce the stress concentration while at the same time keeping safety values for failure criteria. Both Tsai-Wu and LARC03 failure criterion are used in the analyses. In summary, the main contribution of the present work is to show the effectiveness of the proposed generalized fiber parameterization methodology, which is a metaheuristic approach, highlighting the concurrence of mechanical strength and stress concentration in VA composite laminates performance. In addition, it is shown the importance to consider both parameters as objective functions for a multiobjective optimization algorithm for VA composite structures.

2 Proposed Approach: Finite Element Formulation, Fiber Orientation Parameterization and Failure Criteria

In the following subsections, the finite element formulation, the fiber parameterization framework and the failure criteria are presented.

2.1 Finite Element Formulation

An 8-node curved finite element is used in the structural analysis of the variable-stiffness laminated composite shell studied in this work. Ahmad et al. (1970) showed the formulation of this degenerated shell element, which considers first-order shear deformation theory, and Kumar and Palaninathan (1997) extended it to orthotropic materials. This analysis is performed with an in-house software developed in MATLAB (MATLAB 2010). The steps to implement the finite element model can be found in the previously cited references. In this subsection, only topics that are used to construct the fiber parameterization are covered. Figure 1 illustrates a finite element mesh with the nodes, the global coordinate system x_i , the curvilinear natural system ξ_i and the lamina coordinate system e_i , which is assembled at each integration point. The last system is used as a reference for positioning the fibers (the fiber angle at the integration point (θ_{it}) is a measured relative to the e_1 component).

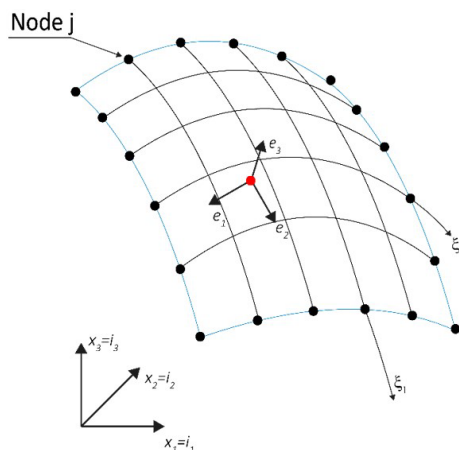


Figure 1: Coordinate systems of the finite element model.

Since the coordinate systems are essential for the construction of the proposed framework, it is important to show some definitions. The \mathbf{e}_3 component is the unit normal vector of the element mid-surface located at a given integration point x_p whose coordinates are obtained using the shape functions of the finite element $N_j(\xi_p)$ as $x_p = x_j N_j(\xi_p)$. This component is calculated as shown in Eq. 1:

$$\mathbf{e}_3 = \frac{\mathbf{x}_{,\xi_1} \times \mathbf{x}_{,\xi_2}}{\|\mathbf{x}_{,\xi_1} \times \mathbf{x}_{,\xi_2}\|}, \tag{1}$$

where, following the procedure developed by Hughes (2000), $\mathbf{x}_{,\xi_1}$ and $\mathbf{x}_{,\xi_2}$ are tangent vectors to the curvilinear natural coordinates ξ_1 and ξ_2 . These intermediate components are obtained as

$$\mathbf{x}_{,\xi_i}(\xi) = \frac{\partial \mathbf{x}(\xi)}{\partial \xi_i} = \mathbf{x}_j \frac{\partial N_j(\xi)}{\partial \xi_i} \quad i=1,2 \tag{2}$$

The remaining components of the coordinate system of the lamina are obtained by a procedure that ensures consistency between the finite elements. This approach certifies that the fiber path is consistent throughout the entire studied structure. The directions defined by the unitary vectors \mathbf{e}_1 and \mathbf{e}_2 are independent of the node numbering order of the elements and \mathbf{e}_1 is parallel to the plane composed by \mathbf{i}_1 and \mathbf{e}_3 and oriented towards the positive direction of the axis x_1 ($\mathbf{e}_1 \cdot \mathbf{e}_2 > 0$), except for a mid-surface perpendicular to the global axis x_1 .

The unit vector \mathbf{e}_2 is oriented in the same direction as the global axis x_2 ($\mathbf{e}_2 = \mathbf{i}_2$), if \mathbf{e}_3 is aligned to the global axis ($\mathbf{x}_1 \parallel \mathbf{e}_3 \cdot \mathbf{i}_1 = 1$). For any other case, \mathbf{e}_2 is obtained as described in Eq. 3.

$$\mathbf{e}_2 = \frac{\mathbf{e}_3 \times \mathbf{i}_1}{\|\mathbf{e}_3 \times \mathbf{i}_1\|} \tag{3}$$

2.2 Fiber Orientation Parameterization

The proposed framework consists of assembling an interpolation function from control points, which are distributed over the area of interest of the structure that has angle values previously assigned angle values. The selected interpolation method is the Radial Basis Function (RBF), which is expressed by

$$\theta_j = \sum_{k=1}^{n_{CP}} \gamma_k \phi(\|\mathbf{x}_j - \mathbf{x}_k\|) + h(\mathbf{x}_j) \tag{4}$$

where $h(\mathbf{x}_j)$ is a polynomial corrector that ensures the uniqueness of the fit and θ_j is the angle interpolated at a node j . The variable γ_k is a weight that is associated with the control point k for the RBF $\phi(\cdot)$, which accumulates the interactions with all surrounding control points as shown by Biancolini (2017).

It is assumed that $\phi(\cdot)$ is conditionally positive definite and h is a linear polynomial. These assumptions allow to obtain the weights vector $\boldsymbol{\gamma}$. The coefficients of the polynomial corrector $\boldsymbol{\beta}$ are obtained in terms of the angles assigned to the control points $\theta_{CP} = \{\theta_1, \dots, \theta_{n_{CP}}\}^T$ by the following system of equations

$$\begin{bmatrix} \mathbf{M} & \mathbf{P}_s \\ \mathbf{P}_s^T & \mathbf{0} \end{bmatrix} \begin{Bmatrix} \boldsymbol{\gamma} \\ \boldsymbol{\beta} \end{Bmatrix} = \begin{Bmatrix} \theta_{CP} \\ \mathbf{0} \end{Bmatrix}, \tag{5}$$

where \mathbf{M} is the interpolation matrix and \mathbf{P} is the constraint matrix described in the literature (Biancolini, 2017). The angles at the integration points θ_{it} are obtained by the interpolation of the nodal angles of a given finite element by using its shape functions as

$$\theta_{it} = \sum_{i=1}^{n_{nodes}} N(\xi, \eta)_i \theta_{node_i} \quad (6)$$

The selected RBF kernel is the thin-plate spline (Eq. 7). In the present work, this kernel was selected since it has not any parameter to be adjusted and it has a variation-diminishing propriety that guarantees some smoothness of the approximations (Buhmann, 2003).

$$\phi(r) = r^2 \log(r) \quad (7)$$

Besides, the software developed by Chirokov (2023) was used to evaluate the radial basis functions obtained in the present work.

2.3 Failure Criteria

Both Tsai-Wu and LARC03 were used as failure criteria in the proposed approach. It is well known that Tsai-Wu failure criterion is very famous compared to LARC03. Therefore, the authors decided to show only the equations for LARC03, keeping in mind the equations of Tsai-Wu.

Davila et al. (2005) considered two main failure modes in the composite material: matrix failures and fiber failures. For matrix failures, a set of criteria based on the concepts proposed by Hashin and Rotem (1973) and the fracture plane proposed by Puck (1998) are applied.

For the matrix under tension and shear stresses (Eq. 8), the fracture planes (α) are normal to the plane of the plies and parallel to the fiber direction.

$$FIM = (1-g) \left(\frac{\sigma_{22}}{Y_{is}^T} \right) + g \left(\frac{\sigma_{22}}{Y_{is}^T} \right)^2 + \left(\frac{\tau_{22}}{S_{is}^L} \right)^2, \quad (8)$$

where Y_{is}^T and S_{is}^L are the *in-situ* matrix strength in tension and *in-situ* longitudinal shear strength presented in Eq (10). In this work, the investigated case studies have thick plies ($h > 0.7$ mm) so g is obtained by

$$g = 1.12^2 \frac{\Lambda_{22}^0}{\Lambda_{44}^0} \left(\frac{Y^T}{S^L} \right)^2 \quad \text{where} \quad \Lambda_{22}^0 = 2 \left(\frac{1}{E_2} - \frac{\nu_{12}^2}{E_1} \right) \quad \text{and} \quad \Lambda_{44}^0 = \frac{1}{G_{12}} \quad (9)$$

and

$$\begin{aligned} Y_{is}^T &= 1.12 \sqrt{2} Y^T \\ S_{is}^L &= \sqrt{2} S^L \end{aligned} \quad (10)$$

If the matrix is under compression and the fiber is under tension, the failure criterion (FI) for the matrix is given by

$$FIM = \left(\frac{\tau_{eff}^m}{S^T} \right)^2 + \left(\frac{\tau_{eff}^L}{S_{is}^L} \right)^2 \quad \text{where} \quad \begin{cases} \tau_{eff}^T = -\sigma_{22} \cos \alpha (\sin \alpha - \eta^T \cos \alpha) \\ \tau_{eff}^L = \cos \alpha (|\tau_{12}| - \eta^L \sigma_{22} \cos \alpha) \end{cases} \quad (11)$$

For this situation, the fracture planes are not necessarily normal to the ply (Equation 11). In this case, the Mohr-Coulomb (Salençon, 2001) effective stresses are used to calculate the angles of the fracture plane. In fact, in Eq. 11, α is the angle of the fracture plane, which is obtained interactively by the maximization of FIM and S^T , which is given by the transverse shear strength presented in Eq. 12. The terms η^T and η^L are the coefficients of transversal and longitudinal influence described in Equation 13. Finally, τ_{eff}^T and τ_{eff}^L are effective stresses in such plane.

$$S^T = Y^C \cos \alpha_0 \left(\sin \alpha_0 + \frac{\cos \alpha_0}{\tan 2\alpha_0} \right), \quad (12)$$

$$\frac{\eta^L}{S^L} = \frac{\eta^T}{S^T}. \quad (13)$$

$$\eta^L = \frac{S^L \cos 2\alpha_0}{Y^C \cos^2 \alpha_0}. \quad (14)$$

The term α_0 in Eq. 14 refers to the typical fracture angle for a laminated composite under transverse compression loading which is 53° while Y^C and S^L are the transversal compression strength and S^L is the longitudinal shear strength. The superscript m refers to imperfections in the fiber alignment that are idealized as a local region of weaviness. The modified stresses for this situation are:

$$\sigma_{22}^m = \cos^2 \varphi \sigma_{11} + \cos^2 \varphi \sigma_{22} - 2 \sin \varphi \cos \varphi |\tau_{12}|, \quad (15)$$

$$\tau_{12}^m = -\sin \varphi \cos \varphi \sigma_{11} + \sin \varphi \cos \varphi \sigma_{22} + (\cos^2 \varphi - \sin^2 \varphi) \tau_{12}, \quad (15)$$

where φ is the sum of a small imperfection angles and rotational components due to shear loading. It is defined as

$$\varphi = \frac{|\tau_{12}| + (G_{12} - X_c) \varphi_c}{G_{12} + \sigma_{11} - \sigma_{22}} \quad (17)$$

and φ_c is the total misalignment angle for the case of pure axial compression loading, described as

$$\varphi_c = \tan^{-1} \left(\frac{1 - \sqrt{1 - 4 \left(S^L / X^C + \eta^L \right) \left(S_{is}^L / X^C \right)}}{2 \left(S_{is}^L / X^C + \eta^L \right)} \right). \quad (18)$$

For fiber in tension, the failure criterion is based on the effective strain acting along the fibers. The noninteracting maximum allowable strain for the LARC03 criterion is defined by:

$$FI_F = \frac{\varepsilon_{11}}{\varepsilon_1^T}, \quad (19)$$

where ε_{11} is the local strain in direction 1 and ε_1^T is the strain strength in this same direction. Finally, for fiber and matrix in compression, the failure criterion yields

$$FI_F = \frac{|\tau_{12}^m| + \eta^L \sigma_{22}^m}{S_{is}^L} \leq 1 \quad (20)$$

while for fiber in compression and matrix into tension, the failure criterion is given by:

$$FI_M = (1 - g) \left(\frac{\sigma_{22}^m}{Y_{is}^T} \right) + g \left(\frac{\sigma_{22}^m}{Y_{is}^T} \right)^2 + \left(\frac{\tau_{12}^m}{S_{is}^L} \right)^2 \quad (21)$$

In summary, Figure 2 shows the main aspects of the proposed optimization procedure and how these topics are linked together. The design variables of the NSGA-II algorithm are angles assigned to the control points (θ_{CP}). These angles are used as a framework to build the radial basis function, which is used to interpolate angles at the finite element nodes. Finally, the shape functions are used to interpolate the nodal angles to the integration points as shown in Figure 3.

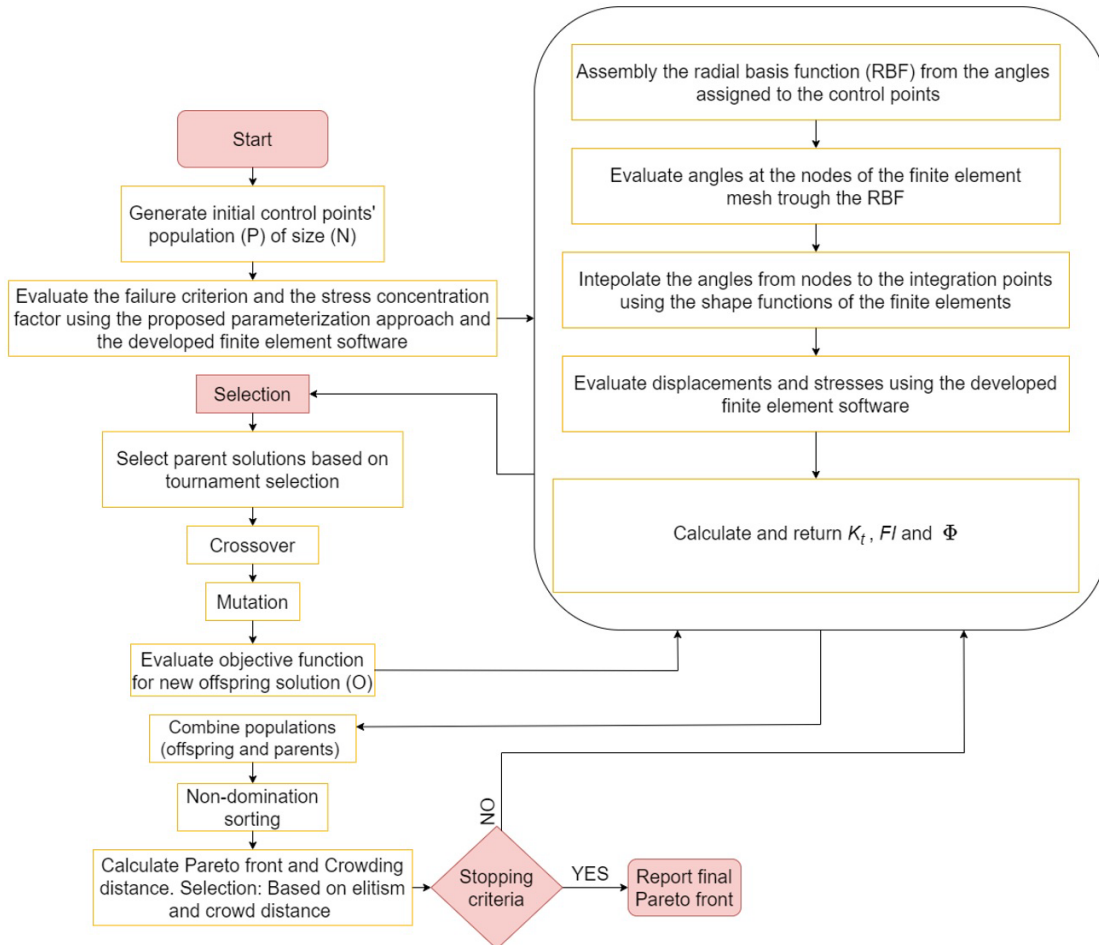


Figure 2: Flowchart of the proposed approach.

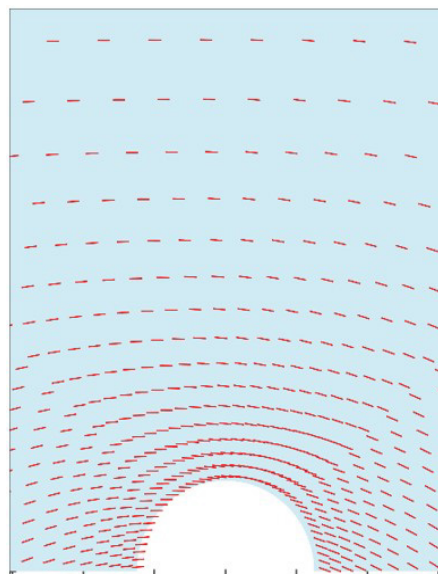


Figure 3: Representation of fiber directions interpolated to the integration points.

3 RESULTS AND DISCUSSION

3.1 Double Notched Plate

The first case study is a composite plate with two notches Weixing and Xinlu (1991). First of all, it was evaluated the developed finite element software to simulate the results obtained in the referenced work. The composite plate in Fig. 4 has only one layer with 5 mm thickness made of Borum/Aluminum. The mechanical elastic properties of this material are $E_1 = 210GPa$, $E_2 = 132GPa$, $\nu_{12} = 0.22$, $G_{12} = 44.8 GPa$. The finite element mesh has 2400 finite elements and its details are also shown in Figure 4.

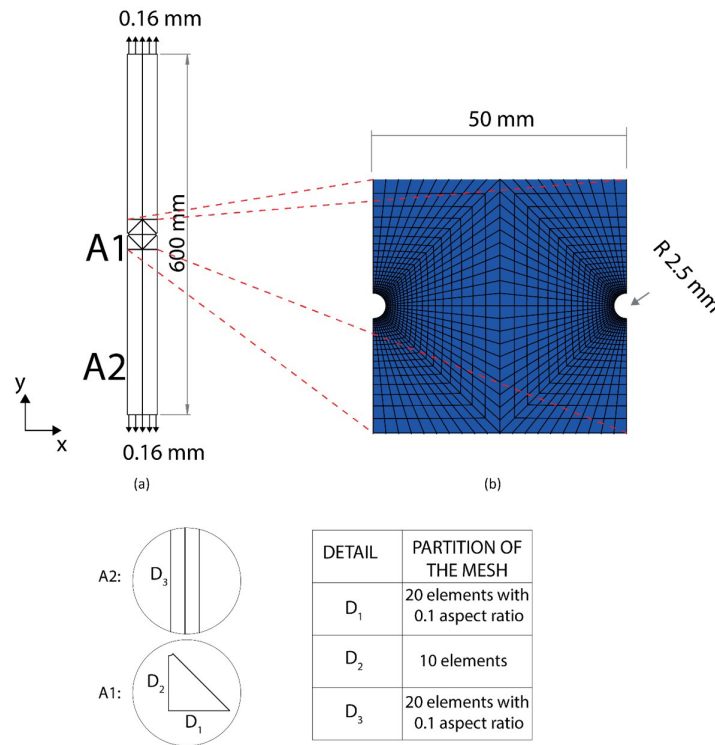


Figure 4: (a) FE mesh details (b) Notch region detail.

The loads consist of prescribed normal displacements of 0.16 mm at the tip edges. The stress concentration factor (K_t) is represented by the ratio between the nominal stress measured at the tip edge of the plate and the maximum stress at the stress concentrator ($K_t = \sigma_n / \sigma_{nominal}$). In fact, the stress components at local direction 1 (aligned to the fibers) are used for this ratio. Weixing and Xinlu (1991) found a value of K_t of 3.6556 for a very refined mesh. In the present work, it was obtained a value of K_t equal to 3.6499 considering the partition of mesh shown in Figure 4. After that, considering the same geometry and loads, it was investigated two different materials as shown in Table 1.

Table 1. Materials mechanical properties and strength values.

Material	E_1 (GPa)	E_2 (GPa)	ν_{12}	G_{12} (GPa)	X^T (MPa)	X^C (MPa)	Y^T (MPa)	Y^C (MPa)	S^L (MPa)
Scotchply 1002	36.8	8.27	0.26	4.14	1062	610	31	1186	72
T300/N5208	181	10.3	0.28	7.17	1500	1500	40	246	68

In Fig. 5, it is possible to observe that nine control points (in blue) were distributed over the finite element mesh, lining off the area of interest, i.e. defining the VA composite region. Only the fibers of the elements contained in the VA composite region can have change in their axis. The remaining domain have their axis direction set to be parallel to the prescribed displacement direction. To maintain the continuity between the elements with variable axis fibers and the unidirectional ones, extra control points (in red) are assigned to the elements, which are neighbors to the VA region (as shown in Figure 5). Thus, the fiber axis directions in the neighbors to the VA region are also parallel to the displacement direction (y axis).

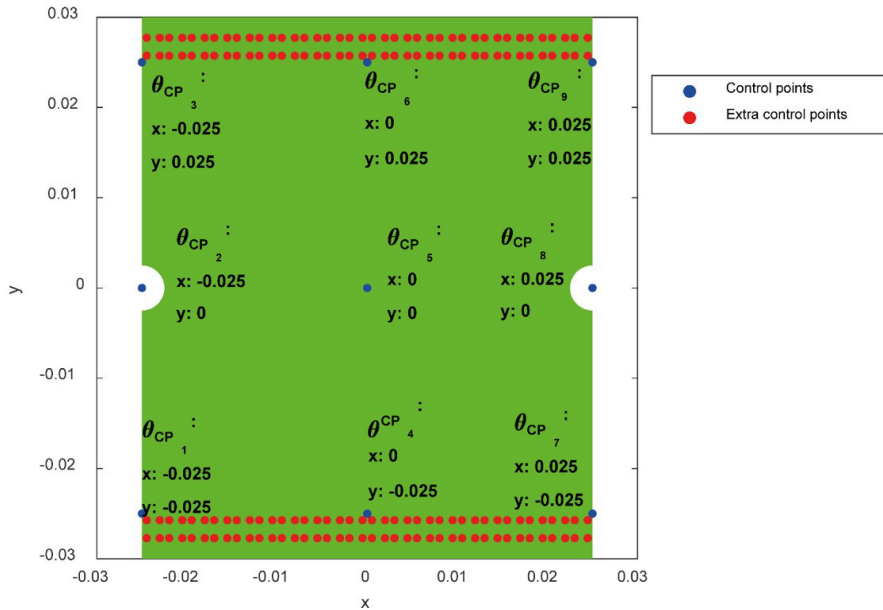


Figure 5: Control points distribution.

The stress values and the failure criterion indices were extrapolated to the nodes using the approach proposed by Hinton and Campbell (1974). The NSGA II software implemented by Song Lin (2023) was used, and a population of 200 individuals and 400 generations were assumed. In Figure 6, Pareto fronts show that the objective functions are concurrent and are suitable to have a multiobjective optimization process.

The obtained numerical results and the values of the fibers angles (or directions of the axis) at the control points are organized in Table 2. In addition, the fibers patterns, maximum principal stress and LARC03 failure criterion indices (FI) for the Scotchply 1002 and T300/N5208 laminate are presented in Figure 6.

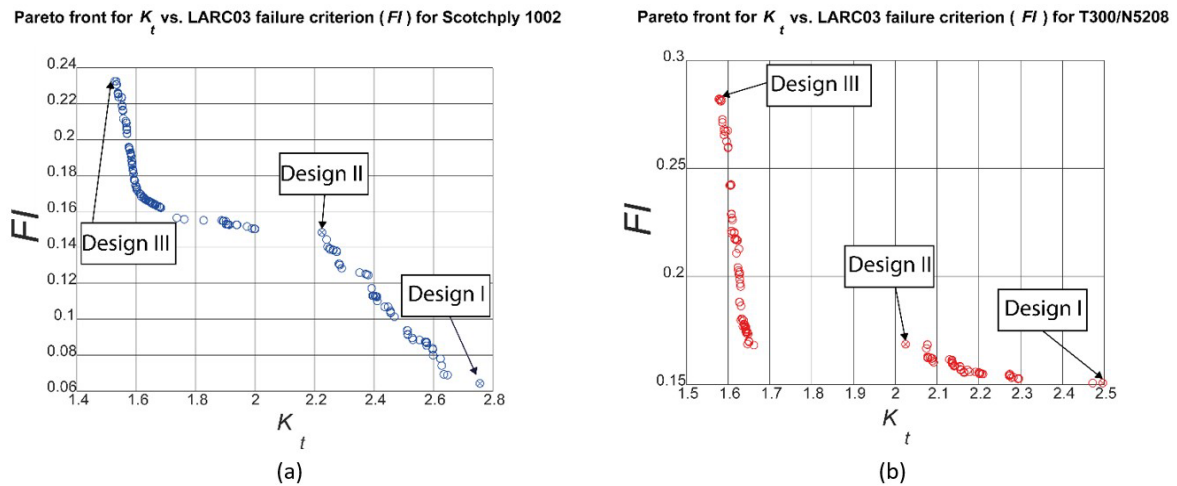


Figure 6: Pareto's front: (a) Scotchply 1002 laminate; (b) T300/N5208 laminate.

Table 2. Design angles (radians) for the obtained fiber paths and results obtained for the double notched plate.

Material		θ_{CP_1}	θ_{CP_2}	θ_{CP_3}	θ_{CP_4}	θ_{CP_5}	θ_{CP_6}	θ_{CP_7}	θ_{CP_8}	θ_{CP_9}	LARC03	K_t
Scotchply 1002	Design I	1.4382	1.6115	1.6704	1.6010	1.3754	1.6045	1.6618	1.6886	1.4324	0.0643	2.7565
	Design II	1.4184	1.0942	1.7884	1.6021	1.4990	1.6068	1.7915	1.0687	1.3760	0.1484	2.2248
	Design III	1.2809	0.4619	1.2369	1.6012	1.4265	1.6021	1.2332	0.4353	1.2576	0.2325	1.5270
T300/N5208	Design I	1.7679	1.9347	1.7101	1.5208	1.5816	1.5637	1.7296	1.4324	1.4514	0.1508	2.4964
	Design II	1.7934	2.1320	1.7261	1.5114	1.5716	1.5775	1.7375	1.8529	1.4069	0.1687	2.0247
	Design III	1.7112	2.1777	1.7798	1.5679	1.4926	1.5637	1.3632	0.7869	1.3317	0.2820	1.5781

For a unidirectional laminate with the fibers aligned with the prescribed displacement, the Scotchply 1002 laminate presents a FI of 0.1183 and a K_t of 4.4619, while the T300/N5208 laminate presented a FI of 0.4239 and a K_t of 5.8469. A maximum reduction of 45.6% and 64.4% in LARC03 failure criterion indices is obtained for Design I using Scotchply 1002 and T300/N5208 laminates, respectively. The maximum reduction in K_t for both laminates is given in Design III, being 66.3% for Scotchply 1002 and 94.2% for T300/N5208.

The same laminate structure is optimized using unidirectional fibers for the same objective function, allowing the comparisons between the obtained results of the resultant VA designs and unidirectional ones. Three additional cases are proposed here: (a) a one-layer plate, (b) a symmetric laminate plate with stack sequence $[\theta_1 / \theta_2 / \theta_2 / \theta_1]$ and (c) a laminate plate with stack sequence $[\theta_1 / \theta_2 / \theta_3 / \theta_4]$. The generated Pareto fronts obtained from the optimization processes executed for these plates are presented in Figure 7, considering that the lateral constraints for the angles are $\mp \frac{\pi}{2}$.

For the one layered plate, the minimum FI was obtained for $[90]$ (all fibers aligned to the y axis, i.e. aligned to the load) and the minimum K_t was obtained for $[0]$. For the symmetric plate, the minimum FI was obtained with a stack sequence $[90/90]_s$ and the minimum K_t with a stacking sequence $[3.94/79.12]_s$. The last proposed stack sequence presents $[90/90/90/90]$ for minimum FI and $[0/49.78/90/88.60]$ for minimum K_t .

The three proposed unidirectional laminates resulted in the same maximum mechanical strength, which was already compared to the obtained VA Design. Based on Figure 7, the single-layered laminate (a) and the symmetric one (b) show similar behavior up to a K_t of 2.67. From this point, the symmetric laminate presents more flexibility, allowing it to reach a K_t of 1.46. Although this Design presents less stress concentration than Design III, it shows a higher penalization in the mechanical strength. The $[\theta_1 / \theta_2 / \theta_3 / \theta_4]$ shows higher flexibility than the one-layered plate and the symmetric laminate (case b). For reduction in the stress concentration factor, from a K_t of 1.67, it is more worthwhile to use the unidirectional fibers since it maintains lower FI and is easier to manufacture.

Pareto fronts for selected unidirectional stack sequences for Scotchply 1002 plates

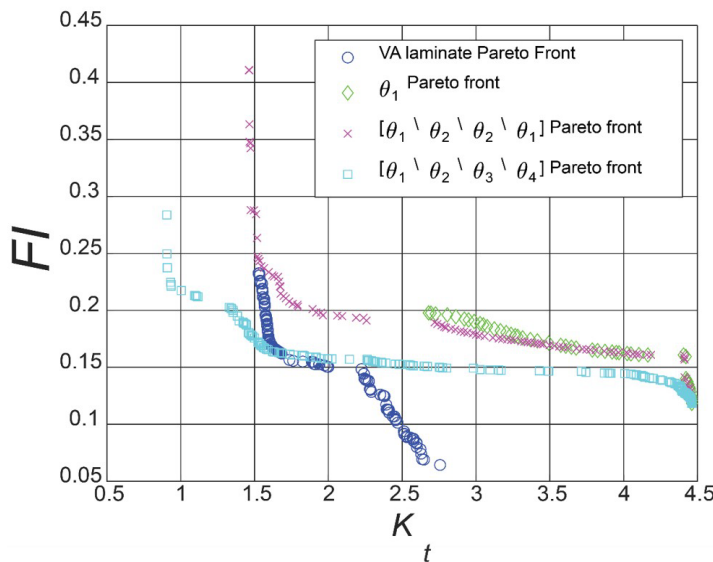


Figure 7: Pareto's fronts: Unidirectional laminates versus VA composites.

In Figure 8, the improvement in the strength for Design I is explained by the fact that the fibers reinforce the structure in x direction near the circular cutout, which is the critical region for failure. At some distance from the circular cutout, the fibers converge to the plate edge, transferring a portion of the load to the matrix, as well as reducing the stress and the K_t . Design II and Design III show that as smaller the K_t , as more acute is the angle of the fibers since they reach the notch. This behavior increases the actuation of the matrix, decreasing the stresses in the notch region while penalizing the mechanical strength.

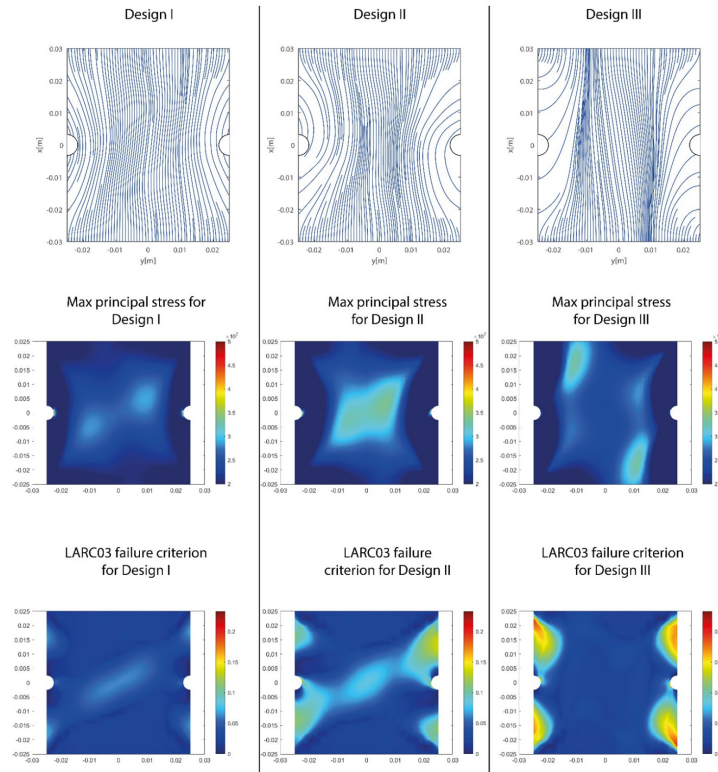


Figure 8: Obtained fiber paths, max stress and failure criterion on the notched region.

3.2 Tube with a transverse hole

This study case is based on the case study presented in Bi et al. (2020). It consists of a tube with a through hole. The tube has a length of 0.8 m with diameter of 0.03 m and the holes have a diameter of 0.01 m. The Scotchply 1002 laminate structure is made of five layers with 1 mm each. The geometry, mesh details and prescribed displacement are shown in Figure 9.

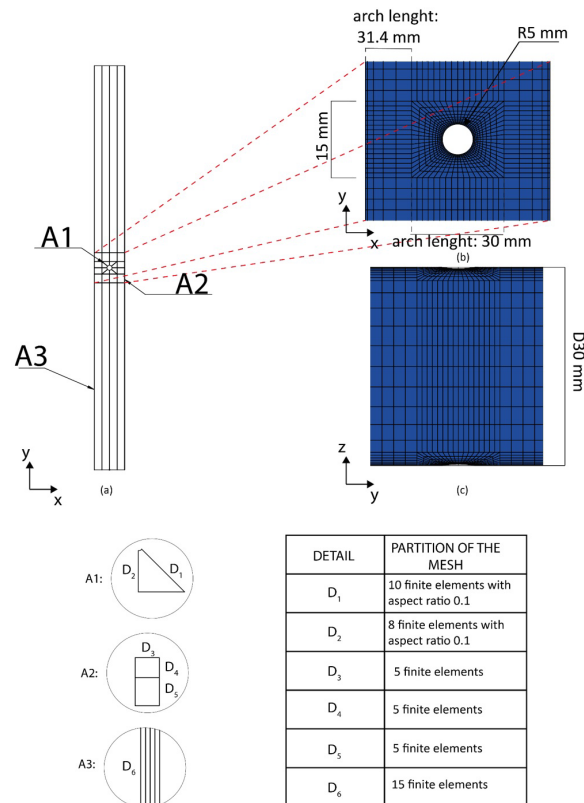


Figure 9: (a) Geometry and FE mesh details. (b) Details of the region of the circular cutout. (c) Lateral view.

In Figure 10, it is possible to observe twelve control points (in blue), which are distributed around the area of interest (VA region). However, as the structure has symmetry, the control points on the lower part of the structure have the same values as the upper one, then for the optimization process, only nine control points remain. The proposed approach was used for the optimization, considering a population of 200 individuals and 200 generations during the analysis.

In addition to the LARC03 criterion, in this case, the application of the Tsai-Wu failure criterion described in Eq. 22 was also investigated.

$$\Phi = \frac{X^C - X^T}{X^C X^T} \sigma_1 + \frac{Y^C - Y^T}{Y^C Y^T} \sigma_2 + \frac{1}{X^C X^T} \sigma_1^2 + \frac{1}{Y^C Y^T} \sigma_2^2 + \frac{1}{X^C X^T Y^C Y^T} \sigma_1 \sigma_2 + \frac{1}{(S^L)^2} \tau_{12} \quad (22)$$

The resulted Pareto fronts for both criteria are presented in Figure 11, and the coefficients generated for the selected designs, as well as their numerical results are presented in Table 3. It is possible to note that both fronts have very similar shapes.

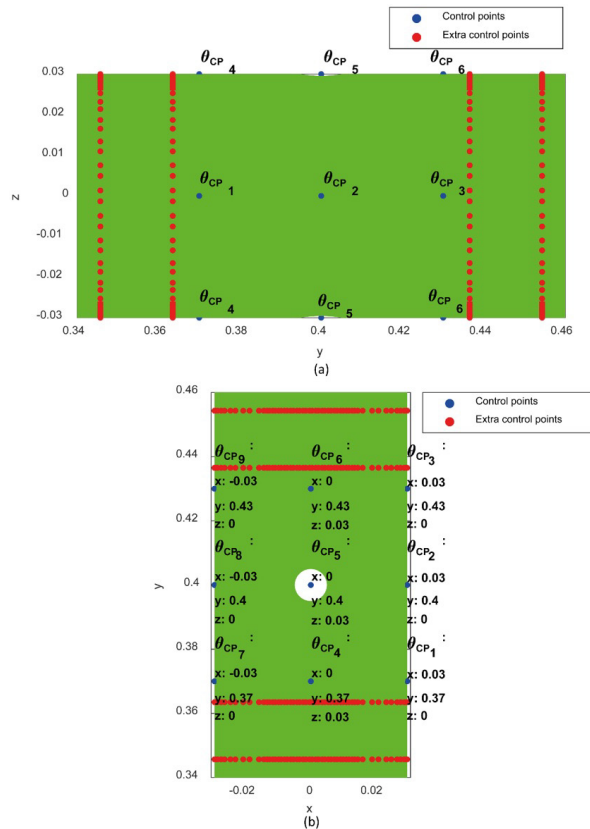


Figure 10: (a) Side view of the cylinder with control points (b) top view of the tube with control points and its coordinates.

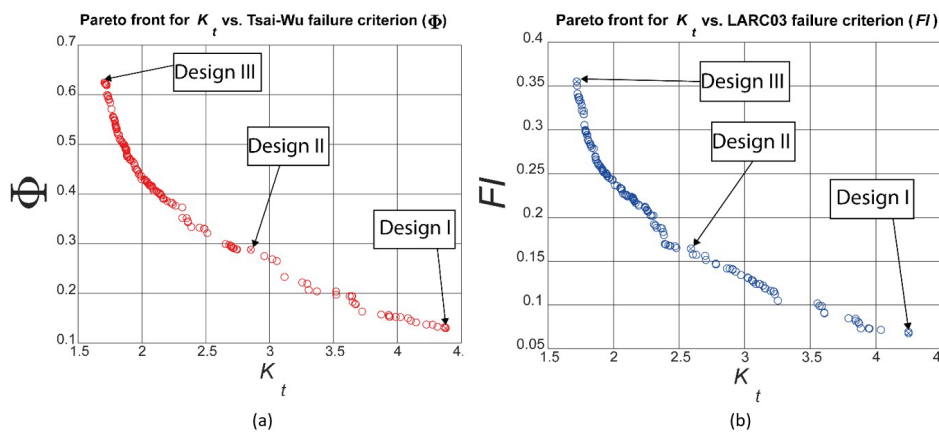


Figure 11: Pareto's front for failure criterion vs. K_t : (a) Tsai-Wu and (b) LARC03 failure criterion.

Table 3. Design angles (radians) for the obtained fiber paths and results obtained for the tube with a transverse hole.

Material		θ_{CP_1}	θ_{CP_2}	θ_{CP_3}	θ_{CP_4}	θ_{CP_5}	θ_{CP_6}	θ_{CP_7}	θ_{CP_8}	θ_{CP_9}	Φ/FI	K_t
Tsai-Wu	Design I	1.7549	1.6770	1.6340	1.0885	1.5611	1.1609	1.8940	1.7311	1.7988	0.1300	4.3778
	Design II	0.9723	0.5071	1.0474	2.4991	2.2191	2.4082	1.2975	0.4308	1.2364	0.2879	2.8529
	Design III	2.6176	-0.7076	2.7075	0.1166	2.8777	0.1704	2.4367	0.4310	2.4826	0.6243	1.7059
LARC03	Design I	1.1153	1.3791	1.2226	2.0893	1.6219	2.0752	1.1925	1.1325	1.2616	0.2820	1.5781
	Design II	0.8918	-0.1020	1.0630	2.2149	2.2799	2.1766	0.8690	-0.2296	0.9583	0.1687	2.0247
	Design III	2.3196	-0.4485	2.3335	0.1656	2.9013	0.3149	2.4506	0.3973	2.3199	0.1508	2.4964

For a unidirectional composite with the fibers aligned to the direction of the displacement, it was obtained a Tsai-Wu failure index of 0.1406 and K_t of 4.8654. Design I is not able to offer a significant improvement (only 7.5%) over the baseline unidirectional laminate showing that, for mechanical strength value, the unidirectional configuration is the best for this laminate. Increasing the number of layers with different fiber paths or studying other control points distributions could expand the solution space and lead to better results. In Figure 12, for Design I, it is noticeable that the fibers are almost straight near the hole, reinforcing the hypothesis that the straight unidirectional baseline design is near the optimal configuration for mechanical strength. In Design II and Design III, the same behavior noted in the previous case was observed with the fibers assuming a certain angle near the hole reducing the portion of the load supported by the fibers and, consequently, decreasing the stress and the mechanical strength in the cutout region.

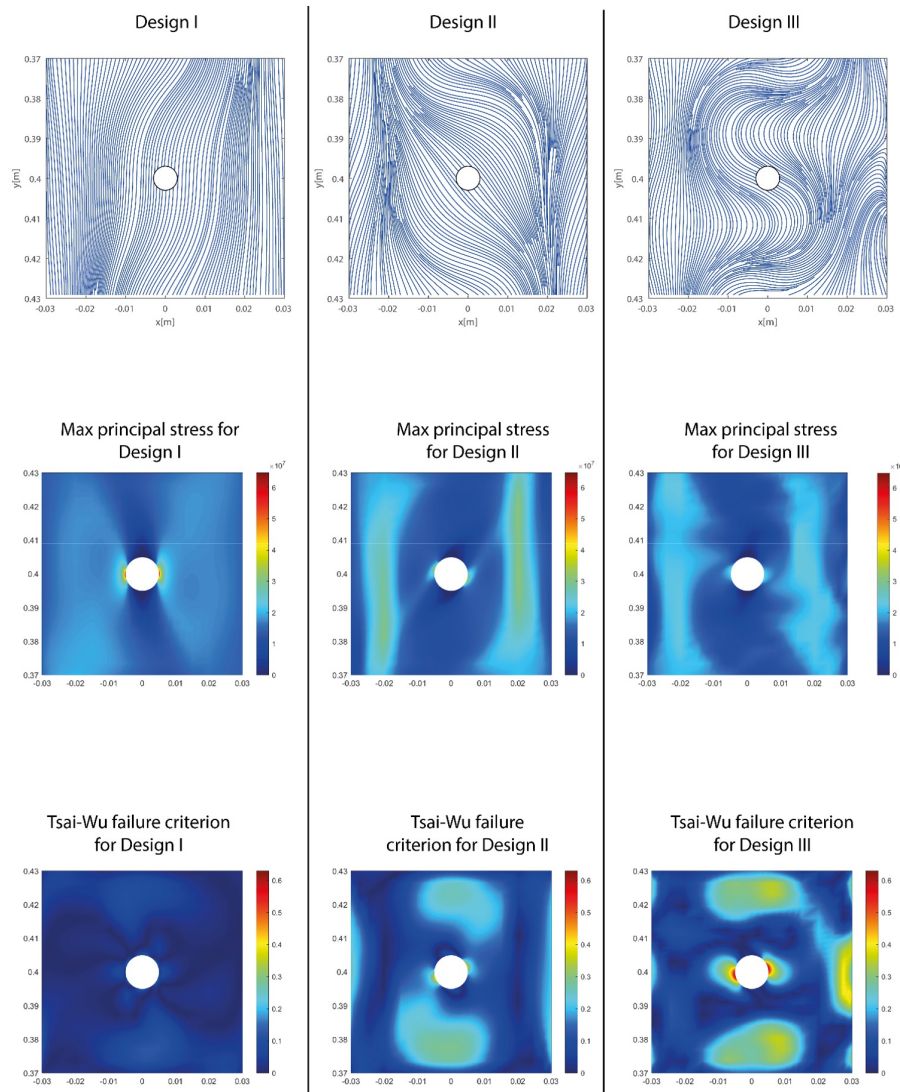


Figure 12: Obtained fiber paths, max stress and failure criterion on the circular cutout region.

In Design I, the Tsai-Wu failure index increases by 104.8%, and the K_t decreases by 34.8%, while in Design II, there is an increment of 344% in the Tsai-Wu failure index, and the K_t decreases by 61.1%. The fibers patterns in this case follow a similar behavior that the one described in the plate, thus it is necessary to have a balance between mechanical strength value (FI) and stress concentration factor (K_t). For LARC03 failure criterion, the unidirectional baseline design has a failure criterion value of 0.0788, and Design I show an improvement of 14% in the mechanical strength value and 12.6% in K_t . This more significant improvement in the failure criterion value is attributed to the accuracy of LARC03 in detecting the failure of the laminate since there are slight differences between fiber paths obtained using each of the failure criteria, as shown in Figure 13.

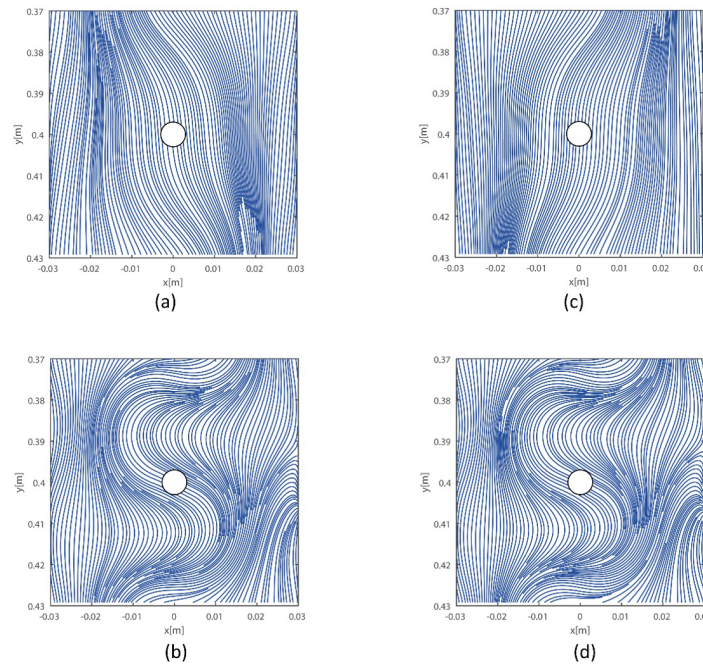


Figure 13: Design I and Design III fiber path for (a,b) LARC03 and (c,d) Tsai-Wu.

4 CONCLUSION

The present paper proposed a framework for multiobjective optimization of VA composites. The stress concentration factor (K_t) and mechanical strength values, or failure criterion (FI), were then explored as objective functions. It was demonstrated that they are suitable (concurrent) for the multiobjective optimization process, resulting in a Pareto's front.

A double notched plate and a tube with holes were investigated. Referring to the plate, when compared to a unidirectional composite laminate where the fibers are aligned to the prescribed displacement, both objective functions are improved for all points of the Pareto's front for the T300/N5208 laminate. Regarding the tube, there is no significant improvement in terms of strength to the unidirectional design, but it was able to reduce the stress concentration close to the holes.

Acknowledgments

Volnei Tita acknowledges the financial support from the National Council for Scientific and Technological Development (CNPq process number: 310159/2022-9), FAPESP-FAPERGS (process number: 2019/15179-2 and 19/2551), as well as Coordenação de Aperfeiçoamento de Pessoal de Nível Superior – Brasil (CAPES-FCT: AUXPE 88881.467834/2019-01) – Finance Code 001. Herbert M. Gomes acknowledges the financial support of the National Council for Scientific and Technological Development (CNPq process number: 301719-2017-9 and 304626-2021-0).

Author's Contributions: PB Santana, Writing – original draft, Visualization, Validation, Software, Methodology, Investigation, Formal analysis, Data curation, Conceptualization; HM Gomes, Writing – re-view & editing, Methodology, Conceptualization; V Tita, Writing – review & editing, Writing – original draft, Supervision, Conceptualization; AJM Ferreira: Writing – review & editing, Writing – original draft, Methodology, Conceptualization.

Editor: Marco L. Bittencourt and Josué Labaki

References

- Ahmad S, Irons BM, Zienkiewicz OC (1970) Analysis of thick and thin shell structures by curved finite elements. *Int J Numer Meth Engng* 2:419–451. <https://doi.org/10.1002/nme.1620020310>
- Alex Chirokov (2023) Scattered Data Interpolation and Approximation using Radial Base Functions
- Almeida JHS, Bittrich L, Jansen E, et al (2019) Buckling optimization of composite cylinders for axial compression: A design methodology considering a variable-axial fiber layout. *Composite Structures* 222:110928. <https://doi.org/10.1016/j.compstruct.2019.110928>
- Almeida JHS, St-Pierre L, Wang Z, et al (2021) Design, modeling, optimization, manufacturing and testing of variable-angle filament-wound cylinders. *Composites Part B: Engineering* 225:109224. <https://doi.org/10.1016/j.compositesb.2021.109224>
- Bi Z, Pilkey WD, Pilkey DF (2020) Peterson's stress concentration factors, Fourth edition. John Wiley & Sons, Inc, Hoboken, NJ
- Biancolini ME (2017) Fast Radial Basis Functions for Engineering Applications. Springer International Publishing, Cham
- Buhmann MD (2003) Radial basis functions: theory and implementations. Cambridge University Press, Cambridge; New York
- Chiang CR (1998) Stress concentration factors of edge-notched orthotropic plates. *The Journal of Strain Analysis for Engineering Design* 33:395–398. <https://doi.org/10.1243/0309324981513093>
- Davila CG, Camanho PP, Rose CA (2005) Failure Criteria for FRP Laminates. *Journal of Composite Materials* 39:323–345. <https://doi.org/10.1177/0021998305046452>
- Guimarães TAM, Pereira DA, Rade DA (2019) Dynamic Behavior and Optimization of Tow Steered Composite Plates. In: Fleury A de T, Rade DA, Kurka PRG (eds) *Proceedings of DINAME 2017*. Springer International Publishing, Cham, pp 169–184
- Hashin Z, Rotem A (1973) A Fatigue Failure Criterion for Fiber Reinforced Materials. *Journal of Composite Materials* 7:448–464. <https://doi.org/10.1177/002199837300700404>
- Hinton E, Campbell JS (1974) Local and global smoothing of discontinuous finite element functions using a least squares method. *Int J Numer Meth Engng* 8:461–480. <https://doi.org/10.1002/nme.1620080303>
- Honda S, Igarashi T, Narita Y (2013) Multi-objective optimization of curvilinear fiber shapes for laminated composite plates by using NSGA-II. *Composites Part B: Engineering* 45:1071–1078. <https://doi.org/10.1016/j.compositesb.2012.07.056>
- Hughes TJR (2000) *The finite element method: linear static and dynamic finite element analysis*. Dover Publications, Mineola, NY
- Jones RM (1999) *Mechanics of composite materials*, 2nd ed. Taylor & Francis, Philadelphia, PA
- Kaw AK (2006) *Mechanics of composite materials*, 2nd ed. Taylor & Francis, Boca Raton, FL
- Kumar WPP, Palaninathan R (1997) Finite element analysis of laminated shells with exact through-thickness integration. *Computers & Structures* 63:173–184. [https://doi.org/10.1016/S0045-7949\(96\)00297-0](https://doi.org/10.1016/S0045-7949(96)00297-0)
- MATLAB (2010) version 7.10.0 (R2010a). The MathWorks Inc., Natick, Massachusetts
- Puck A (1998) FAILURE ANALYSIS OF FRP LAMINATES BY MEANS OF PHYSICALLY BASED PHENOMENOLOGICAL MODELS. *Composites Science and Technology* 58:1045–1067. [https://doi.org/10.1016/S0266-3538\(96\)00140-6](https://doi.org/10.1016/S0266-3538(96)00140-6)
- Salençon J (2001) *Handbook of Continuum Mechanics*. Springer Berlin Heidelberg, Berlin, Heidelberg
- Santana PB, Gomes HM, de Almeida FS, Tita V (2023) A new approach to optimize variable axial composite shells: A metaheuristic procedure using the finite element method. *Thin-Walled Structures* 183:110389. <https://doi.org/10.1016/j.tws.2022.110389>
- Setoodeh S, Abdalla MM, Gürdal Z (2006) Design of variable-stiffness laminates using lamination parameters. *Composites Part B: Engineering* 37:301–309. <https://doi.org/10.1016/j.compositesb.2005.12.001>
- Sobhani Aragh B, Borzabadi Farahani E, Xu BX, et al (2021) Manufacturable insight into modelling and design considerations in fibre-steered composite laminates: State of the art and perspective. *Computer Methods in Applied Mechanics and Engineering* 379:113752. <https://doi.org/10.1016/j.cma.2021.113752>
- Song Lin (2023) NGPM -- A NSGA-II Program in Matlab v1.4

Stodieck O, Cooper JE, Weaver PM, Kealy P (2017) Aeroelastic Tailoring of a Representative Wing Box Using Tow-Steered Composites. *AIAA Journal* 55:1425–1439. <https://doi.org/10.2514/1.J055364>

Ueng CES, Lin J (1987) Stress Concentrations in Composite Laminates. *J Eng Mech* 113:1181–1193. [https://doi.org/10.1061/\(ASCE\)0733-9399\(1987\)113:8\(1181\)](https://doi.org/10.1061/(ASCE)0733-9399(1987)113:8(1181))

van Zanten FJ, Pupo CR, Barazanchy D, Van Tooren MJ (2019) Optimization of 3D Curved Fiber Steered Shells. In: *AIAA Scitech 2019 Forum*. American Institute of Aeronautics and Astronautics, San Diego, California

Vijayachandran AA, Waas AM (2022) Minimizing stress concentrations using steered fiberpaths and incorporating realistic manufacturing signatures. *International Journal of Non-Linear Mechanics* 146:104160. <https://doi.org/10.1016/j.ijnonlinmec.2022.104160>

Wang Z, Almeida Jr. JHS, St-Pierre L, et al (2020) Reliability-based buckling optimization with an accelerated Kriging metamodel for filament-wound variable angle tow composite cylinders. *Composite Structures* 254:112821. <https://doi.org/10.1016/j.compstruct.2020.112821>

Weixing Y, Xinlu Y (1991) Stress concentration factor for an orthotropic finite-width plate containing elliptical edge notches. *Composites Science and Technology* 41:47–53. [https://doi.org/10.1016/0266-3538\(91\)90051-P](https://doi.org/10.1016/0266-3538(91)90051-P)